Zhao *et al. J Wood Sci* (2021) 67:54
https://doi.org/10.1186/s10086-021-01986-4

Journal of Wood Science

ORIGINAL ARTICLE

Open Access

Mechanical performance of aluminum reinforced wood plastic composites under axial tension: an experimental and numerical investigation

Longlong Zhao[1*], Fei Xi[2] and Xiaorui Wang[3]

Abstract

Wood plastic composites (WPCs) are low-cost biomass composite materials with good mechanical stability and good weather resistance that are mainly used in the areas with low stress levels. Aimed at improving the mechanical properties of WPCs, this paper proposes a new WPC reinforced with aluminum. The WPC and aluminum were hot pressed to form an aluminum reinforced wood plastic composites (A-WPC). The axial tensile properties, stress–strain relationship, and failure mechanism of the composite were studied experimentally. The results show that the ultimate stress and strain, elastic modulus, and other mechanical parameters of A-WPCs are much higher than those of WPCs. The elongation at break is 10.13 times that of WPCs, which greatly improves the ductility. Based on the equivalent stiffness theory, two calculation models were proposed to predict the tensile stress–strain relationship of A-WPCs. The tensile rebound process of A-WPCs was analyzed in depth, and then the calculation formula of the residual curvature was deduced to compare with the test results. The experimental results are in good agreement with the calculation results.

Keywords: Aluminum reinforced wood plastic composites, Stress–strain relationship, Equivalent stiffness, Tensile springback characteristics

Introduction

Wood plastic composites (WPCs) are green and environment-friendly biomass composites [1–3], which has a wide range of raw materials, low production cost, nice-looking, and good weatherability. WPCs are widely used in indoor and outdoor decorations, landscape architecture, the automobile field, packaging and transportation, and other fields that require low mechanical properties [4]. In recent years, many studies have been completed to enhance the mechanical properties of WPCs and expand the application field of WPCs. Migneault et al. [5] and Kumari et al. [6] found that the mechanical properties of WPCs produced by an injection molding process were better than those produced by hot pressing and extrusion molding. The mechanical properties of WPCs were greatly improved when *p*-toluenesulfonic acid (*p*-TsOH) was used as a compatible coupling agent by Lin et al. [7] to remove hemicellulose from wood flour to change the cross-sectional compatibility of the WPC. Rimdusitet al. [4], Petchwattana et al. [8], Tao et al. [9], Perisicet al. [10], and Panaitescu et al. [11] tested different toughening agents to improve the impact strength, tensile elongation at break, and other mechanical properties of WPCs. Many experiments have investigated improving the mechanical properties of WPCs with carbon fiber [12], glass fiber [13], basalt fiber [14], polyester fiber [15], and mineral wool. However, no reinforcement

*Correspondence: nlzll@njfu.edu.cn
[1] College of Civil Engineering, Nanjing Forestry University, Nanjing 210037, China
Full list of author information is available at the end of the article

measures can significantly improve the strength, elastic modulus, and ductility at the same time. This paper proposes a new reinforced measure by exploiting the light weight, high strength, and good ductility of aluminum to improve the mechanical properties of WPCs. The WPC and aluminum are hot pressed into an aluminum reinforced wood plastic composite (A-WPC). Experimental investigation of the tension behavior of the A-WPC has been carried out. The equivalent stiffness method is used to calculate the elastic modulus of the strengthened composite. Based on this, two sets of calculation models of the uniaxial tensile stress–strain relationship of the A-WPC are proposed to predict the load carrying capacity and stress–strain relationship of the new composite, which can provide a theoretical basis for the design and calculation of a building structure composed of A-WPCs.

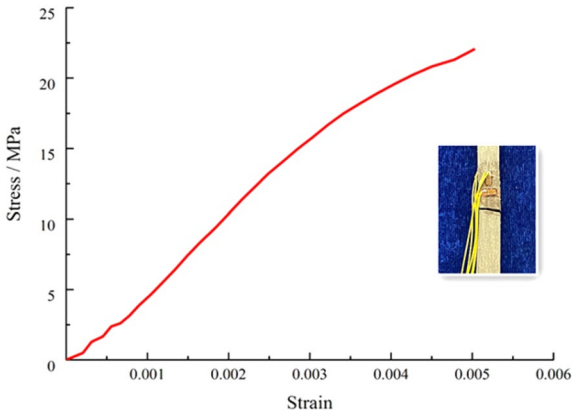

Fig. 1 Stress–strain relationship of the WPC

Experimental tests

Materials

The raw WPC material used in this study was composed of 30% polyolefin, 50% wood flour (60 mesh), and 15% calcium carbonate. The tensile trial samples were produced by Anhui Sentai Co., Ltd, Anhui province, China. The tensile test of the WPC was carried out according to ASTM d-143 [16]. Six specimens were tested on the electronic universal testing machine. The longitudinal and transverse strains in the middle of the specimen and the homologous real-time load were collected throughout the experiment. Table 1 lists the test results, where σ_{tu} is the ultimate stress, ε_{tu} infers the ultimate strain, E_t represents the elasticity modulus, A implies the elongation at fracture, and v is the Poisson's ratio. As shown in Fig. 1, the stress–strain relationship exhibits a linear character, and no obvious plasticity occurs until the specimen was damaged, implying the characteristics of brittle failure.

The aluminum alloy was made by hot rolling in Sentai Co., Ltd. The test design and operation were performed according to ASTM E8-E8M [17], and the number of aluminum samples was also 6. The measured parameters were consistent with the WPC tensile test, and the results are shown in Table 1. Comparing the test results with those of the WPC, the ultimate tensile strength, elastic modulus, ultimate strain, and elongation at break of the aluminum plate are 9.5 times, 10.4 times, 6 times, and 20.9 times those of the WPC, respectively, while the Poisson's ratio of the two materials is substantially identical.

Table 1 Mechanical parameters of WPC and aluminum

	σ_{tu}/MPa	A/%	v	E_t/GPa	ε_{tu}/%
WPC					
Average value	21.29	0.61	0.35	6.09	0.0045
Standard deviation	1.02	0.074	0.016	0.20	0.00045
CoV	4.81	12.12	4.47	3.30	10.13
Aluminum					
Average value	201.48	12.74	0.35	63.62	0.027
Standard deviation	5.41	1.49	0.016	2.34	0.0023
CoV	2.69	11.68	4.52	3.67	8.51

CoV coefficient of variation

In Fig. 2, the stress–strain relationship of the aluminum tensile test is different from that of the WPC, which has an obvious specific elastic limit point. When the curve reaches the elastic–plastic stage, the increasing rate of stress decreases relative to the increasing rate of strain, forming a yield platform. Then, the strain increases, but the stress is almost unchanged in this stage, which demonstrates the good ductility of aluminum. The failure sections are obviously necking, and they are all oblique sections. In addition, the angle between the section and sample cross axis is about 30°, as shown in Fig. 2.

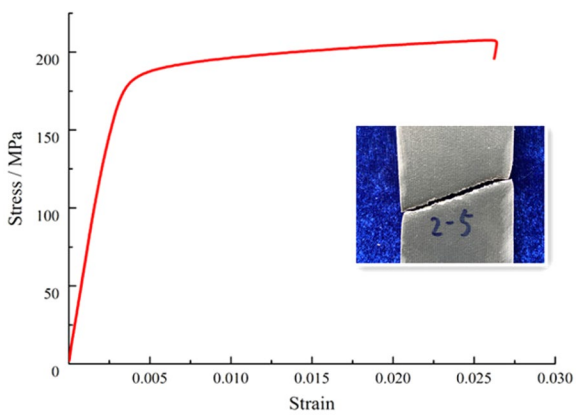

Fig. 2 Stress–strain relationship of aluminum

Sample design

A 1.5 mm thick aluminum was first pulled into the pattern die by the hauling machine, and then the 2.5 mm thick WPC was attached to the aluminum surface by the co-extrusion machine on the side of the pattern die. The aluminum reinforced wood plastic composite plate with a thickness of 4 mm is finally formed by hot pressing (the temperature is 160–200 °C and the pressure is 20 MPa). The A-WPC tensile samples were processed based on ASTM E8-E8M [17]. The sample number is 1–1–1–6, the overall length is 450 mm, the gauge length is 200 mm, and the width is 40 mm.

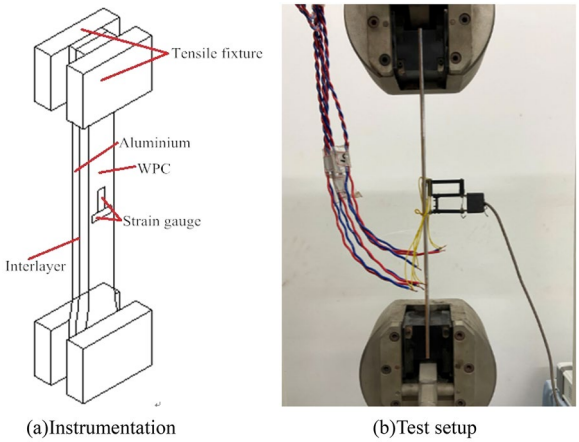

Fig. 3 Test setup and instrumentation

Test scheme

As shown in Fig. 3a, the tensile fixtures were selected to hold the grip sections of the specimen. One longitudinal and one transverse perpendicular strain gauge were arranged on the two sides of the middle part of the sample to measure the strain in the tensile direction and perpendicular to the tensile direction during the test. In Fig. 3b, the tensile experiment of the A-WPC was carried out on a 50 kN electronic universal testing machine. The applied load was recorded simultaneously. The loading mode is crossbeam stroke control, and the loading rate is 0.5 mm/min. All load and strain data were collected by the Data Logger TDS-530(Tokyo Sokki Kenkyujo Co., Ltd., Japan), and the sampling frequency was 1 Hz.

Test results and discussion

Test results

As shown in Fig. 4a, all the specimens are damaged at the effective part, that is, the part with the smallest cross section of the sample. Unlike the aluminum test results, the failure section of the A-WPC is almost parallel to the horizontal axis of the sample, and no obvious necking is observed, as shown in Fig. 4b. This indicates that the WPC can effectively prevent the aluminum from necking when bearing a uniaxial tensile load. After the failure of the specimens, they all bent towards the WPC and

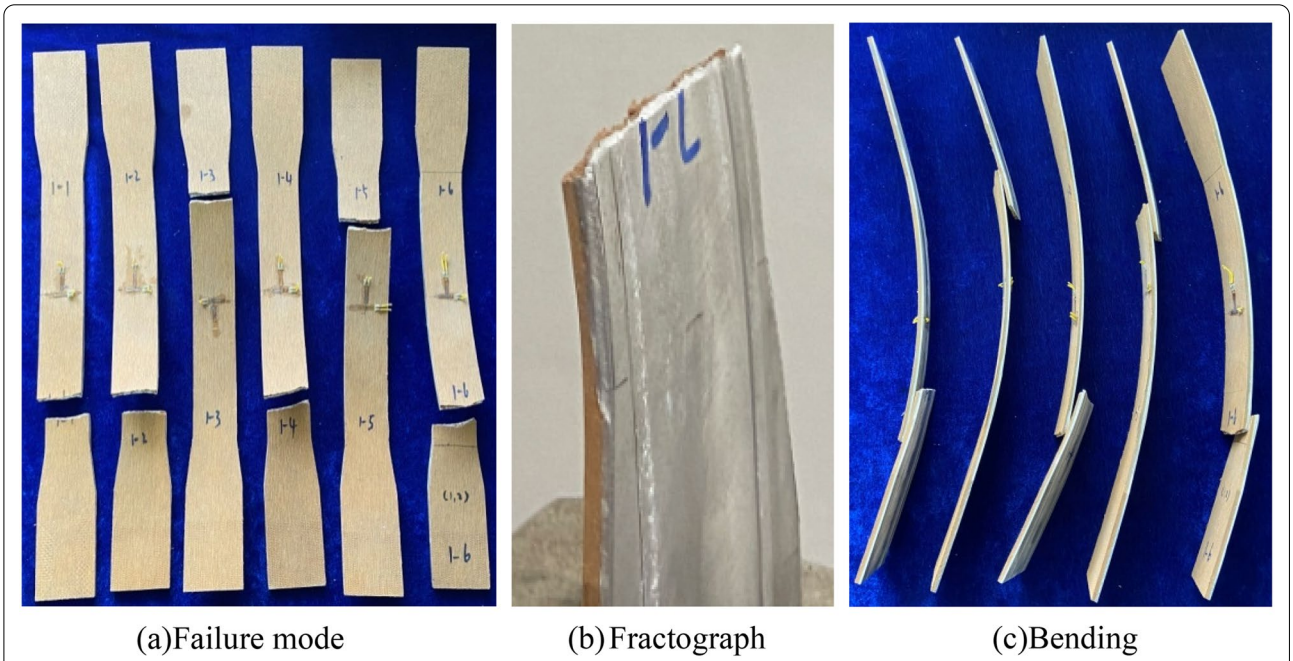

Fig. 4 Phenomenon of destruction

Table 2 Test results

	σ_{tu}/MPa	*A*/%	*v*	E_t/GPa	ε_{tu}/%
1–1	86.01	6.23	0.33	24.43	0.018
1–2	82.16	5.40	0.36	25.61	0.018
1–3	81.60	6.69	0.38	23.93	0.015
1–4	84.35	7.46	0.37	24.67	0.018
1–5	86.49	5.89	0.36	25.13	0.016
1–6	83.83	5.40	0.33	23.28	0.015
Average value	84.070	6.17	0.35	24.51	0.017
Standard deviation	1.80	0.73	0.019	0.83	0.0015
CoV	2.14	11.82	5.33	3.40	8.8

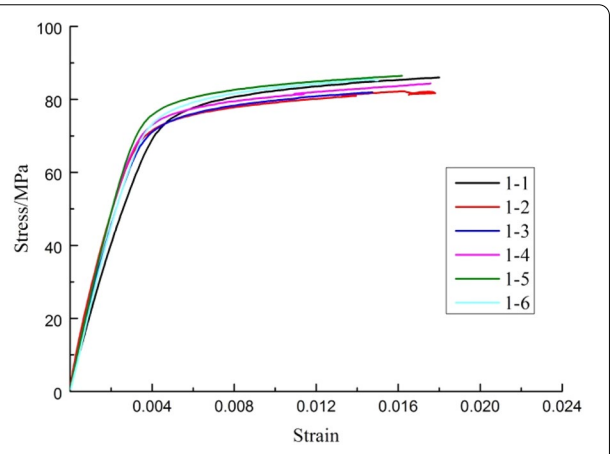

Fig. 5 Tensile stress–strain relationship of the A-WPC

formed into arcs, as shown in Fig. 4c. Different elastic modulus lead to the unequal residual strains of the two materials after fracture springback, resulting in bending deformation of the whole sample.

The experimental results of the A-WPC are shown in Table 2. The coefficient of variation of all the parameters is less than 17%, meeting the specification requirements. Meanwhile, only the coefficient of variation of the elongation at break is more than 10%, which is 12%. The R^2 of the ultimate strength and elastic modulus are less than 5%, which shows that the A-WPC continues to exhibit the advantages of good homogeneity, stable mechanical properties, and low dispersion of the WPC.

Figure 5 shows the tensile stress–strain relationship of the A-WPC, which can be divided into three stages: elastic stage, elastic–plastic stage, and ductile failure stage. At first, the relationship between the stress and strain is linear. After reaching the proportional limit, the slope of the curve becomes smaller, and the curve enters the elastic–plastic stage. In this stage, the growth rate of stress decreases relative to the growth rate of strain, and finally, it enters the ductile failure stage. At this time, the strain increases continuously, the stress increases slowly, and the sample undergoes a large deformation, which displays brilliant ductility until the sample fails.

Calculation model

Equivalent elastic modulus

The Poisson's ratio of the WPC and aluminum is consistent, which possesses the basic elements of deformation coordination, and no relative slip appears in the tensile process of the A-WPC, indicating that the A-WPC has good mechanical stability. Thus, the equivalent stiffness method can be used to calculate the elastic modulus of the A-WPC, as shown in the following equation:

$$E = \frac{E_{\mathrm{W}} w t_{\mathrm{w}} + E_{\mathrm{A}} w t_{\mathrm{A}}}{w t_{\mathrm{w}} + w t_{\mathrm{A}}} = \frac{E_{\mathrm{W}} t_{\mathrm{w}} + E_{\mathrm{A}} t_{\mathrm{A}}}{t_w + t_{\mathrm{A}}}, \tag{1}$$

where E_{W} (E_{A}) and t_{W} (t_{A}) are the elastic modulus and the thickness of the WPC (aluminum), respectively, and w is the width of the sample. By substituting the elastic modulus of the WPC and aluminum into Eq. (1), the calculated value of the elastic modulus of the A-WPC is 27.66 GPa, which is different from the experimental result by only 12.8%.

Model I—bilinear model

The elastic–plastic stage, as the transition section between the elastic and the ductile failure stage, can be decomposed into the extended section of the elastic stage and the initial stage of the ductile failure section. Then, the stress–strain relationship can be disassembled into two linear curves. The slope of the first straight line is the elastic modulus, and the slope of the curve drops sharply after reaching the inflection point strength; therefore, the bilinear model including two straight lines can be written as the following equation:

$$f = \begin{cases} E\varepsilon & 0 < \varepsilon \le \varepsilon_{\mathrm{ey}} \\ \sigma_{\mathrm{ey}} + kE\left(\varepsilon - \varepsilon_{\mathrm{ey}}\right) & \varepsilon_{\mathrm{ey}} < \varepsilon \le \varepsilon_{\mathrm{u}} \end{cases}, \tag{2}$$

where σ_{ey} and $\varepsilon_{\mathrm{ey}}$ are the inflection point strength and homologous strain of the A-WPC, respectively, which is between the proportional limit and yield strength point, and k is a constant. According to the tensile test results, by setting the inflection point strength to be 90% of the ultimate strength, the inflection point strain is the strain corresponding to the inflection point strength, and k is suggested to be 0.03. Substituting the above parameters into Eq. (2):

$$f = \begin{cases} 24510\varepsilon & 0 < \varepsilon \le 0.0031 \\ 75.98 + 735(\varepsilon - 0.0031) & 0.0031 < \varepsilon \le 0.017 \end{cases}. \tag{3}$$

Figure 6 shows the fitting results of the A-WPC tensile stress–strain bilinear model. The model is simple in form and easy for hand computation. The two segments can well describe the stress–strain relationship at different stages and can also predict the elastic modulus, ultimate strength, and ultimate strain of the materials accurately.

Model II—exponential model

In the light of the tensile test characteristics of the A-WPC, the exponential function model (Eq. 4) is introduced to predict the tensile stress–strain relationship:

$$f(x) = \frac{\sigma}{\sigma_y} = e^{bx} - e^{dx}, \tag{4}$$

where $x = \varepsilon/\varepsilon_y$, σ_y and ε_y represent the yield stress and yield strain, respectively, and b and d are constants that can be obtained from the test results. Equation (4) is derived, and $x = 0$ is taken into Eq. (5), where E is the elastic modulus and E_{sec} is the secant modulus of the yield point:

$$b - d = \frac{E}{E_{sec}}. \tag{5}$$

Substituting the test results into Eq. (5) for the calculation and setting σ_y to be 95% of the ultimate strength, ε_y is the strain corresponding to the yield point. After regression analysis, we suggest that $b = 0.02$ and $d = -1.55$. Taking these parameters into Eq. (4), the expression of the tensile stress–strain relationship of the A-WPC can be obtained as

$$\sigma = 79.91\left(e^{6.06\varepsilon} - e^{-469.7\varepsilon}\right). \tag{6}$$

Figure 7 shows that the trend of the stress–strain relationship between the exponential model and the test results of the A-WPC is almost the same, which means this model can describe the whole process of the stress–strain relationship development. When the numerical simulation and software analysis of the A-WPC are carried out, the exponential model can get more accurate results.

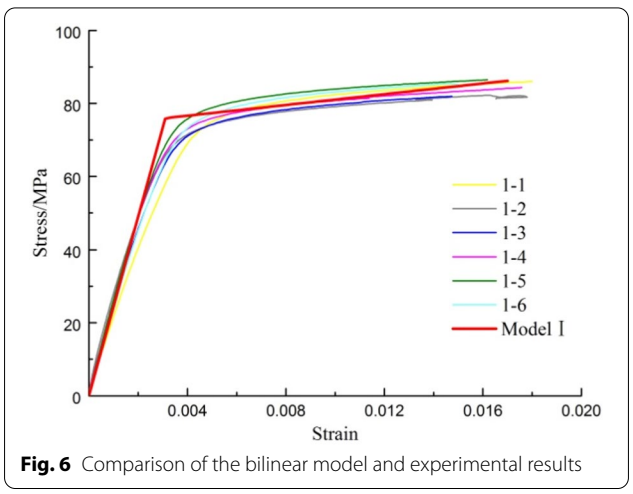

Fig. 6 Comparison of the bilinear model and experimental results

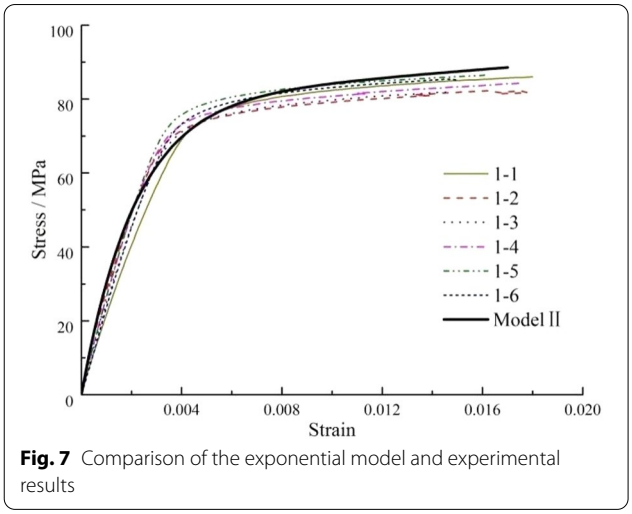

Fig. 7 Comparison of the exponential model and experimental results

Analysis of tensile springback of the A-WPC

Throughout the experiment, no interface relative slip and interface delamination occurred in all specimens, which indicates that the WPC and aluminum are in a state of coordinated deformation in the whole process of the trial. The eccentric tensile load and additional bending moment can be ignored, and the tensile process can be regarded as a plane stress state. As shown in Fig. 8, the tensile springback process of the A-WPC is as follows: assuming that the original length of the sample is L, the length after the uniaxial tensile load is $L + 2\delta_u$, and the tensile strain of the sample is ε_u, when unloading, the sample begins to shrink and spring back, and bending occurs. The springback is divided into the

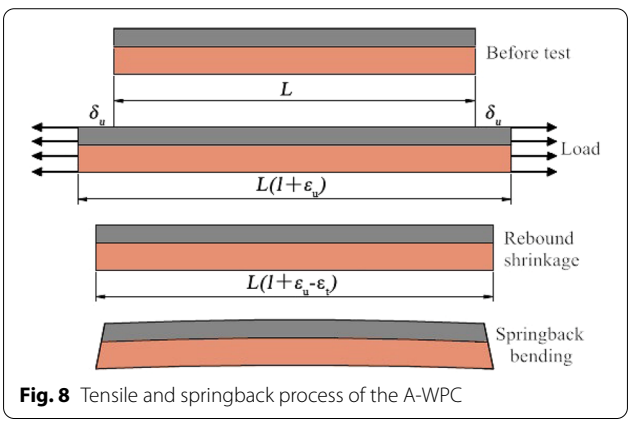

Fig. 8 Tensile and springback process of the A-WPC

springback shrinkage stage and the springback bending stage. Supposing that the sample only shrinks and does not bend in the springback shrinkage stage, the sample will rebound until the resultant stress of the section is 0. Then, in the springback bending stage, the sample will bend under the action of the pure bending moment, the stress of the section will redistribute, and the final bending moment of the section will be 0.

Let us assume that the constitutive relationship of the aluminum and WPC can be described by the bilinear model, which is divided into the elastic section and linear strengthening section. In this model, E_a, E_a', σ_{ay}, ε_{ay}, and t_a are the elastic value of the aluminum elastic section, the elastic modulus of the linear strengthening section, the yield strength, the yield strain, and the thickness, respectively. The corresponding parameters of the WPC are E_w, E_w', σ_{wy}, ε_{wy}, and t_w, where $\varepsilon_{ay}=\sigma_{ay}/E_a$ and $\varepsilon_{wy}=\sigma_{wy}/E_w$. The thickness of the A-WPC is $t=t_a+t_w$, the actual thickness coordinate is h, the section residual strain is $\varepsilon_c(h)$, and the bending residual curvature is $A=\varepsilon_c(h)/h$.

When the longitudinal section with a residual strain of 0 is defined as the neutral axis of the residual strain, the offset of the neutral axis from the interface is δ. When the tensile strain is defined as ε_k, the stress of the aluminum is σ_{ak} and the stress of the WPC is σ_{wk}; when the rebound strain is defined as ε_t, the stress of the aluminum is σ_{at} and the stress of the WPC is σ_{wt}; the residual stress is $\varepsilon_c(z)$.

When the tensile strain is ε_k, the stresses of the WPC and aluminum could be expressed by Eqs. (7) and (8):

$$\sigma_{wk}=\begin{cases} E_w\varepsilon_k & \varepsilon_k \le \varepsilon_{wy} \\ E_w\varepsilon_{wy}+E_w'(\varepsilon_k-\varepsilon_{wy}) & \varepsilon_k > \varepsilon_{wy} \end{cases}. \tag{7}$$

$$\sigma_{ak}=\begin{cases} E_a\varepsilon_k & \varepsilon_k \le \varepsilon_{ay} \\ E_a\varepsilon_{ay}+E_a'(\varepsilon_k-\varepsilon_{ay}) & \varepsilon_k > \varepsilon_{ay} \end{cases}. \tag{8}$$

When the springback strain is ε_t, the stresses of the aluminum and WPC follows:

$$\begin{cases} \sigma_{at}=\sigma_{ak}-E_a\varepsilon_t \\ \sigma_{wt}=\sigma_{wk}-E_w\varepsilon_t \end{cases}. \tag{9}$$

There is no bending of the A-WPC during the springback shrinkage stage. When the resultant force of the internal force of the section is 0, there is the following relationship: $t_a\sigma_{at}+t_w\sigma_{wt}=0$. Taking Eq. (9) into it leads to the following equation:

$$\varepsilon_t=\frac{t_a\sigma_{ak}+t_w\sigma_{wk}}{t_aE_a+t_wE_w}. \tag{10}$$

The internal moment M_t can be expressed as Eq. (11):

$$M_t=\frac{t_a^2}{2}(\sigma_{ak}-E_a\varepsilon_t)+\frac{t_w^2}{2}(\sigma_{wk}-E_w\varepsilon_t). \tag{11}$$

Under a pure bending load, the distance between the strain neutral axis and the interface is δ, and the rotation angle of the section relative to the z-axis is θ (δ and θ can be positive or negative). Under this condition, the bending normal stress of the aluminum is σ_{ab} and that of the WPC is σ_{wb}. The strain distribution of the pure bending section of the A-WPC is shown in Fig. 9.

Supposing that θ is small enough, now the strain distribution function along the z-axis is

$$\varepsilon(z)=\tan\theta(z-\delta). \tag{12}$$

The strain is replaced by tan θ $(z-\delta)$, and the bending normal stress could be expressed as

$$\begin{cases} \sigma_{wB}=E_w\tan\theta(z-\delta) & 0<z\le t_w \\ \sigma_{aB}=E_a\tan\theta(z-\delta) & -t_a<z\le 0 \end{cases}. \tag{13}$$

The resultant force of the pure bending normal stress distribution along the section is 0, that is, the sum of the bending normal stress of the A-WPC along the z-axis is 0, as shown in the following equation:

$$\int_0^{t_w}\sigma_{wB}dz+\int_{-t_a}^{0}\sigma_{aB}dz=0. \tag{14}$$

Taking Eqs. (13) into (14), δ can be determined by the following equation:

$$\delta=\frac{E_wt_w^2+E_at_a^2}{2(E_wt_w-E_at_a)}. \tag{15}$$

When the bending moment produced by the bending normal stress on the section is M, then Eq. (14) becomes

$$\int_0^{t_w}\sigma_{wB}dz+\int_{-t_a}^{0}\sigma_{aB}dz=M. \tag{16}$$

Then, taking Eq. (13) into Eq. (16), we can figure out the expression of tanθ:

$$\tan\theta=\frac{M}{E_w\left(\frac{1}{3}t_w^3-\frac{1}{2}\delta t_w^2\right)-E_a\left(\frac{1}{3}t_a^3+\frac{1}{2}\delta t_a^2\right)} \tag{17}$$

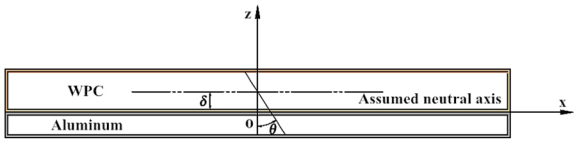

Fig. 9 Section strain distribution

If $M=-M_t$, the transformation process of the section stress is considered to be the process of the bending moment M_t formed in the springback shrinkage stage and further releasing of the bending moment, i.e., the rebound bending stage. The superposition of the two stress states determined by Eqs. (9) and (13) is the residual stress state of the section after tensile springback. The residual curvature of the A-WPC can be regarded as the curvature caused by the bending moment M_t. According to the definition of the residual curvature and Eq. (12), $A \approx \tan\theta/2$ can be calculated. By substituting Eqs. (5) and (11) into $A \approx \tan\theta/2$, the final residual curvature of the A-WPC can be expressed as

$$A=\frac{t_a^2(\sigma_{ak}-E_a\varepsilon_t)+t_w^2(\sigma_{wk}-E_w\varepsilon_t)}{4\left[E_a\left(\frac{t_a^3}{3}+\frac{\delta}{2}t_a^2\right)-E_w\left(\frac{t_w^3}{3}-\frac{\delta}{2}t_w^2\right)\right]}. \tag{18}$$

Substituting the test results into Eqs. (10) and (15), the springback strain and the offset of the neutral axis relative to the interface are calculated as $\varepsilon_t=0.0033$ and $\delta=-1.13$ mm, respectively. Then, taking the above two results into Eq. (18), $A=0.28/m^{-1}$ can be calculated. The residual strain difference of the test results of the samples labelled as 1–1–1–6 is brought into the formula $A=\varepsilon_c(h)/h$. The results are illustrated in Fig. 10, indicating that the average residual curvature of the tensile springback of the WPC aluminum composite plate is $0.31/m^{-1}$, which is 9.7% higher than the theoretical value. This means that Eq. (18) can accurately predict the tensile springback curvature of the A-WPC.

Comparison of the mechanical properties between the A-WPC and WPC

Figure 11 shows the ratio of the mechanical parameters of the tensile test of the A-WPC to the WPC, including ultimate strength, ultimate strain, elastic modulus, Poisson's ratio, and elongation at break. The ratio of the ultimate strength, ultimate strain, elastic modulus, and elongation at break is 3.95, 3.7, 4.03, and 10.13, respectively, while the Poisson's ratio of the A-WPC is almost equal to that of the WPC.

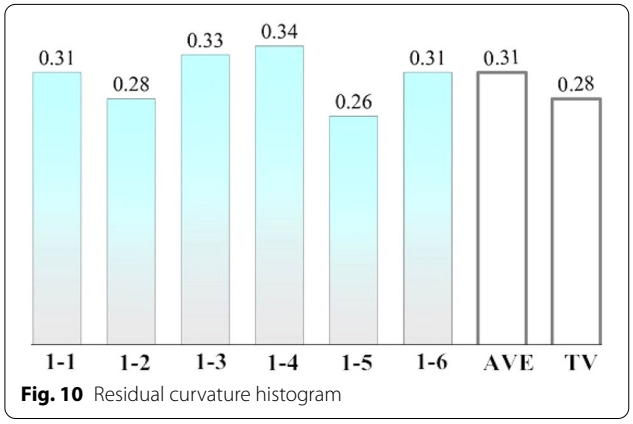

Fig. 10 Residual curvature histogram

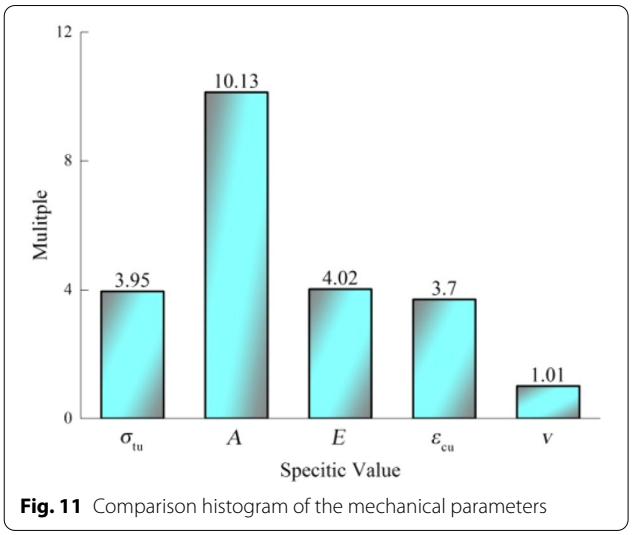

Fig. 11 Comparison histogram of the mechanical parameters

The results show that the ultimate strength, elastic modulus, and especially the elongation at break of the WPC are mainly enhanced by the aluminum, which indicates that the stiffness, strength, and ductility of the WPC can be significantly improved by hot pressing the WPC and aluminum. This approach fixes the problem that no reinforcement measures can significantly improve the strength, elastic modulus, and ductility at the same time.

Conclusion

The Poisson's ratio of the WPC is close to that of the aluminum, making it possible for the two materials to deform cooperatively without relative slip. Only one of the coefficients of variation of the measured mechanical properties is higher than 10%, which indicates that the mechanical properties of the reinforced WPC(A-WPC) are stable and the dispersion is small.

The strength, stiffness, and the elongation at break of the WPC are significantly enhanced, which indicates that the A-WPC can overcome the issue that no reinforcement measures can improve the strength, elastic modulus, and ductility simultaneously. These results change the current situation that WPC sare only used in the field with lower requirements for the mechanical properties.

The springback process of the A-WPC can be divided into the springback shrinkage and rebound bending stage. According to the critical state, the equilibrium equation was established, and the theoretical calculation formula of the residual curvature was obtained. The

difference between the calculation results and the experimental results is within 10%.

The equivalent stiffness principle was used to calculate the elastic modulus of the A-WPC, and two calculation models were established to predict the stress–strain relationship. The appropriate model could be selected according to the actual demand.

Abbreviations
WPC: Wood plastic composite; A-WPC: Aluminum reinforced wood plastic composite.

Acknowledgements
The authors gratefully acknowledge the support by Nanjing University of Finance & Economics and Sentai WPC Group Co., Ltd.

Authors' contributions
Under supervision by FX, LZ performed the sample preparation and data analysis. LZ developed the mechanics modeling and analysis. LZ performed the sample preparation and structure fabrication. XW performed the calculations. All authors contributed to the manuscript. All authors read and approved the final manuscript.

Funding
Youth Project of Natural Science Foundation of Jiangsu Province of China (BK20190796), the General Project of Philosophy and Social Sciences of Jiangsu Province of China (2020SJA0256), the Boutique Project of Social Science Applied Research of Jiangsu Province of China(19SYC-133).

Availability of data and materials
Some or all of the data, models, or code generated or used during the study are available from the corresponding author by request.

Declarations

Competing interests
The authors declare that they have no competing interests.

Author details
[1]College of Civil Engineering, Nanjing Forestry University, Nanjing 210037, China. [2]College of Materials Science and Engineering, Nanjing Forestry University, Nanjing, China. [3]Jiangsu Long-Leaping Engineering Design Co., Ltd., Nanjing, China.

Received: 26 May 2021 Accepted: 14 September 2021
Published online: 23 September 2021

References

1. Li G, Lao W, Qin T, Huang L (2015) Rapid determination of biomass and polypropylene in three types of wood plastic composites (WPCs) using FTIR spectroscopy and partial least squares regression (PLSR). Holzforschung 69:339–404
2. Basalp D, Tihminlioglu F, Sofuoglu SC, Inal F, Sofuoglu A (2020) Utilization of municipal plastic and wood waste in industrial manufacturing of wood plastic composites. Waste Biomass Valori 11:5419–5430
3. Rowell RM (2007) Challenges in biomass-thermoplastic composites. J Polym Environ 15(4):229–235
4. Rimdusit S, Wongsongyot S, Jittarom S, Tiptipakorn SS (2011) Effects of gamma irradiation with and without compatibilizer on the mechanical properties of polypropylene/wood flour composites. J Polym Res 18:801–809
5. Migneault S, Koubaa A, Erchiqui F, Chaala EK, Wolcott, (2009) Effects of processing method and fiber size on the structure and properties of woodplastic composites. Compos A Appl Sci Manuf 40(1):80–85
6. Kumari R, Ito H, Takatani M, Uchiyama M, Okamoto T (2007) Fundamental studies on wood/cellulose-plastic composites: effects of composition and cellulose dimension on the properties of cellulose/PP composite. J Wood Sci 53:470–480
7. Lin H, Li R, Li D, Huang Z, Pang J, Zhang X, Liu W, Yang W (2020) Hydrophobic wood flour derived from a novel p -TsOH treatment for improving interfacial compatibility of wood/HDPE composites. Cellulose 27:4053–4065
8. Petchwattana N, Covavisaruch S (2014) Mechanical and morphological properties of wood plastic biocomposites prepared from toughened poly(lactic acid) and rubber wood sawdust (*Hevea brasiliensis*). J Bionic Eng 11:630–637
9. Tao Q, Yu D, Gao H, Wang Y (2012) Polylactide-based wood plastic composites toughened with SBS. Polym-Plast Technol 51:193–198
10. Perisic SD, Radovic I, Petrovic M, Marinkovic A, Radojevic V (2017) Processing of hybrid wood plastic composite reinforced with short PET fibers. Mater Manuf Process 33:572–579
11. Panaitescu DM, Nicolae CA, Gabor AR, Trusca R (2020) Thermal and mechanical properties of poly(3-hydroxybutyrate) reinforced with cellulose fibers from wood waste. Ind Crop Prod 145:112071
12. Vaentsi O, Kaerki T (2014) Utilization of recycled mineral wool as filler in wood-polypropylene composites. Constr Build Mater 55:220–226
13. Valente M, Sarasini F, Marra F, Tirillo J (2011) Pulci G (2011) Hybrid recycled glass fiber/wood flour thermoplastic composites: manufacturing and mechanical characterization. Compos Part Aappl S 42(6):649–657
14. Almaadeed MA, Kahraman R, Khanam PN, Madi N (2012) Date palm wood flour/glass fibre reinforced hybrid composites of recycled polypropylene: mechanical and thermal properties. Mater Design 42:289–294
15. Chen J, Teng ZY, Wu JJ (2017) Recycling of waste FRP and corn straw in wood plastic composite. Polym Compos 38:2140–2145
16. ASTM D 143-14 (2014) Standard test methods for small clear specimens of timber. ASTM International, Pennsylvania
17. ASTM E8/E8M-16a (2016) Standard test methods for tension testing of metallic materials. ASTM International, Pennsylvania

Publisher's Note